Journal of Applied Analysis and Computation
Volume 17, Number 1, February 2027, 608–631
Website:http://www.jaac-online.com
DOI:10.11948/20250056

BIFURCATIONS AND EXACT SOLUTIONS IN A NONLINEAR SCHRÖDINGER EQUATION WITH HIGH-ORDER NONLINEARITY*

Sumin Yang[1], Yuanyuan Tan[2,†] and Liang Zhao[3]

Abstract This paper investigates the dynamics of a nonlinear Schrödinger equation (NLSE) featuring seventh-order nonlinearity and weak nonlocality. By reducing the governing equation to a planar Hamiltonian system, we perform a systematic qualitative analysis and provide a complete topological classification of its phase portraits. In contrast to previous studies that derived specific chirped solitary waves using ansatz-based methods, our approach employs the bifurcation theory of dynamical systems to uncover the full spectrum of more than 42 distinct exact bounded solutions. These include not only smooth periodic and solitary waves but also non-smooth localized structures such as peakons, periodic peakons, and compactons. We provide explicit parametric representations for each wave profile and establish the parametric conditions under which they emerge. Our results provide a comprehensive map of the localized structures admitted by this high-order NLSE model.

Keywords Homoclinic solution, heteroclinic solution, peakons and periodic peakons, nonlinear Schrödinger equation.

MSC(2010) 34C07, 34D10, 37G20.

1. Introduction

The nonlinear Schrödinger equation (NLSE) and its various generalizations constitute one of the most fundamental models in nonlinear science, with applications spanning nonlinear optics, Bose–Einstein condensates, plasma physics, and water wave theory [37]. In the context of nonlinear optics, the propagation of ultrashort optical pulses in media with competing nonlinearities has attracted sustained attention, as higher-order nonlinear effects become non-negligible when the incident intensity is sufficiently large. In particular, nonlocal nonlinearity—where the wave-induced refractive index change at a given point depends on the field intensity in its neighborhood—introduces novel physical effects that cannot be captured by purely local models.

Recently, Messouber et al. [26] investigated the dynamics of light beams in a weakly nonlocal medium exhibiting nonlinearities up to the seventh order. The governing equation is the

†The corresponding author.
[1]Department of Basic Education, Hangzhou Polytechnic, Hangzhou, Zhejiang 311100, China
[2]China-ASEAN Institute of Statistics, Guangxi University of Finance and Economics, Nanning, Guangxi 530000, China
[3]School of Mathematics, Nanning Normal University, Nanning, Guangxi 530000, China
*Supported by the Funds of the Hangzhou Polytechnic (HKYZXKP-2026-3) and the Natural Science Foundations of China (12461031).
Email: smyang125@126.com(S. Yang), tyygxef@gxufe.edu.cn(Y. Tan), zhaoliang200809@yeah.net(L. Zhao)

following higher-order NLSE:

$$i\psi_z + \alpha\psi_{xx} + \gamma\psi|\psi|^2 + \nu\psi|\psi|^4 + \psi|\psi|^6 + \mu\psi(|\psi|^2)_{xx} = 0, \tag{1.1}$$

where ψ represents the complex amplitude of the electric field, z is the propagation distance, and x denotes the transverse spatial coordinate. Here, α is the diffraction coefficient, γ and ν are the coefficients of the cubic and quintic nonlinearities, respectively, and the term involving μ accounts for weak nonlocality. Equation (1.1) incorporates polynomial nonlinearity up to the seventh order, making it a natural extension of the standard cubic-quintic NLSE. The qualitative theory of dynamical systems has been widely employed to study exact traveling wave solutions of nonlinear PDEs; for instance, Li and Shi [19] recently used the planar dynamical systems approach to investigate traveling wave solutions of *abcd*-water wave models, obtaining a rich variety of exact bounded parametric representations.

To find exact solitary wave solutions of equation (1.1), Messouber et al. [26] adopted a chirped traveling wave ansatz of the form

$$\psi(z,x) = \rho(\xi)\exp(i(\kappa z - \Omega x + \theta(\xi))), \tag{1.2}$$

where κ and Ω represent the propagation constant and frequency shift, respectively, and $\xi = x - qz$ is a traveling coordinate with q denoting the transverse velocity of the wave. The real-valued functions ρ and θ describe the amplitude and phase modulation along the traveling wave. As noted in [26], while chirp-free bright soliton solutions on a zero background for the model (1.1) had been obtained under a special parametric condition in [37], the underlying envelope equation (1.1) had not been solved exactly in its full generality. The approach of Messouber et al. led to chirped localized bright and gray solitary waves via a special solution method. However, this leaves open the important question: What is the complete spectrum of traveling wave solutions admitted by the reduced dynamical system, and how do these solutions depend on the intrinsic system parameters?

In this paper, we address this question by taking a complementary perspective—the bifurcation theory of planar dynamical systems. Substituting the ansatz (1.2) into equation (1.1) and separating the real and imaginary parts, we obtain the following system of ordinary differential equations:

$$(\alpha + 2\mu\rho^2)\rho'' + 2\mu\rho(\rho')^2 - (\kappa + \alpha\Omega^2)\rho - \alpha(\theta')^2\rho + (2\Omega\alpha + q)\theta'\rho + \gamma\rho^3 + \nu\rho^5 + \rho^7 = 0 \tag{1.3}$$

and

$$\alpha\theta''\rho + 2\alpha\theta'\rho' - (2\Omega\alpha + q)\rho' = 0, \tag{1.4}$$

where $'$ denotes the derivative with respect to ξ. From equation (1.4), we readily obtain

$$\theta' = \frac{q + 2\alpha\Omega}{2\alpha} + \frac{C}{2\alpha\rho^2}, \tag{1.5}$$

with C being an integration constant. Substituting (1.5) into (1.3) yields

$$(\alpha + 2\mu\rho^2)\rho'' + 2\mu\rho(\rho')^2 + \left(\Omega q - \kappa + \frac{q^2}{4\alpha}\right)\rho - \frac{C^2}{4\alpha\rho^3} + \gamma\rho^3 + \nu\rho^5 + \rho^7 = 0. \tag{1.6}$$

Equation (1.6) is equivalent to the following planar dynamical system:

$$\frac{d\rho}{d\xi} = y, \quad \frac{dy}{d\xi} = -\frac{2\mu\rho y^2 + \left(\Omega q - \kappa + \frac{q^2}{4\alpha}\right)\rho - \frac{C^2}{4\alpha\rho^3} + \gamma\rho^3 + \nu\rho^5 + \rho^7}{\alpha + 2\mu\rho^2}, \tag{1.7}$$

which is an eight-parameter system depending on the parameter vector $(\alpha, \gamma, \nu, \mu, \kappa, \Omega, q, C)$. This system admits a rich variety of dynamical behaviors and possesses the first integral

$$H(\rho, y) = y^2(2\mu\rho^2 + \alpha) + \left(\frac{C^2}{4\alpha\rho^2} + \left(\frac{q^2}{4\alpha} - \kappa + q\Omega\right)\rho^2 + \frac{1}{2}\gamma\rho^4 + \frac{1}{3}\nu\rho^6 + \frac{1}{4}\rho^8\right) = h. \tag{1.8}$$

To uncover exact solutions of equation (1.1), we set $C = 0$ in (1.7) and focus on the reduced system

$$\frac{d\rho}{d\xi} = y, \quad \frac{dy}{d\xi} = -\frac{2\mu\rho y^2 + b_0\rho + \gamma\rho^3 + \nu\rho^5 + \rho^7}{\alpha + 2\mu\rho^2} \equiv \frac{-\rho(2\mu y^2 + f(\rho^2))}{\alpha + 2\mu\rho^2}, \tag{1.9}$$

with the corresponding first integral

$$H(\rho, y) = y^2(2\mu\rho^2 + \alpha) + \left(b_0\rho^2 + \frac{1}{2}\gamma\rho^4 + \frac{1}{3}\nu\rho^6 + \frac{1}{4}\rho^8\right) = h, \tag{1.10}$$

where $b_0 = \Omega q - \kappa + \frac{q^2}{4\alpha}$ and $f(s) = b_0 + \gamma s + \nu s^2 + s^3$. For each fixed real number h, the level curve defined by (1.10) is an eighth-degree algebraic curve, whose geometric properties encode the full spectrum of bounded traveling wave solutions.

Remark on the case $C \neq 0$. When $C \neq 0$, equation (1.7) contains a singular term $-C^2/(4\alpha\rho^3)$, which introduces an essential singularity at $\rho = 0$ and substantially complicates the dynamical analysis. In particular, the origin $O(0,0)$ is no longer an equilibrium point of system (1.7), and the Hamiltonian (1.8) acquires a term $C^2/(4\alpha\rho^2)$ that blows up as $\rho \to 0$, rendering the level curves qualitatively different from those studied in the present paper. The $C \neq 0$ case corresponds physically to traveling waves with non-trivial phase chirp (cf. (1.5)), and its analysis would require a separate investigation using techniques for singular perturbations or blow-up methods. For this reason, the present work focuses on the chirp-free case $C = 0$, which already yields a remarkably rich variety of bounded traveling wave profiles, leaving the $C \neq 0$ case for future work.

When $\mu\alpha < 0$, system (1.9) constitutes a singular traveling wave system of the first kind, as defined by Li and Chen [17]. Singular traveling wave systems are characterized by the presence of singular straight lines in the phase plane, which give rise to non-smooth wave phenomena such as peakons, compactons, and periodic peakons—features that are absent in smooth Hamiltonian systems. Over the past three decades, nonlinear wave equations admitting non-smooth solitary wave solutions have attracted considerable attention from both physicists and mathematicians. The term "peakon" was first introduced by Camassa and Holm [4, 5] in the context of the celebrated Camassa–Holm equation, and subsequently, numerous integrable peakon equations have been discovered and intensively studied, including the Degasperis–Procesi equation [7, 8], the Qiao equation [28, 29], and the Novikov equation [27]. The systematic bifurcation theory for singular traveling wave systems was developed in [16, 17] and the references therein. More recently, He, Zhang, and Tang [14] studied the orbital stability of the sum of N peakons for the coupled Camassa–Holm and modified Camassa–Holm equation, further advancing our understanding of peakon dynamics in multi-component systems.

A peakon is a peaked soliton whose first-order spatial derivative is discontinuous at the peak, while the wave profile itself remains continuous. More precisely, the profile of a wave function is called a peakon if, at a point of continuity, its left- and right-hand derivatives are finite but opposite in sign (see [9]). Peakons, periodic peakons, and pseudo-peakons are all remarkable examples of non-smooth traveling wave solutions of nonlinear partial differential equations (PDEs). The existence and classification of such solutions are intimately connected with the bifurcations and dynamical behaviors of the associated traveling wave ODE systems. Consequently, the qualitative theory of planar dynamical systems—in particular, the method of phase portrait analysis—provides a powerful and geometrically transparent framework for uncovering the complete menu of bounded traveling wave solutions. This reduction from PDE to planar Hamiltonian ODE via a traveling wave ansatz, combined with bifurcation analysis, has been successfully applied across a broad class of nonlinear wave equations. For instance, Sun and Zhang [34] recently employed a similar approach together with Abelian integral theory to investigate the solitary and periodic traveling waves of a quartic KdV equation with multiple dissipation terms, establishing existence conditions through degenerate Hopf, homoclinic, and Poincaré bifurcations. Furthermore, the same general methodology—converting an infinite-dimensional PDE into a finite-dimensional near-Hamiltonian system on an invariant manifold—has been applied to the complex cubic-quintic Ginzburg–Landau equation with higher-order dispersion via Melnikov analysis [33], further highlighting the versatility of this framework.

Once a parametric representation of $\rho(\xi)$ is obtained from the analysis of system (1.9), a corresponding solution to the original PDE (1.1) is reconstructed via

$$\psi(z,x) = \rho(x-qz)\exp\left(i\left(\kappa z - \Omega x + \frac{q+2\alpha\Omega}{2\alpha}(x-qz)\right)\right). \tag{1.11}$$

While the approach in [26] identified specific chirped bright and gray solitons using a direct ansatz method, it was inherently limited to particular solution types under restricted parametric conditions. Mathematically, the present work provides a significant advancement by transitioning from the search for isolated solutions to a global topological classification of the entire traveling wave system. By employing the bifurcation theory of planar dynamical systems, we provide a complete map of all possible bounded orbits in the phase plane. This systematic perspective allows us to uncover a much broader spectrum of more than 42 distinct solution types—including not only the smooth solitons previously discussed but also a rich variety of non-smooth localized structures such as peakons, periodic peakons, sawtooth waves, and compactons—which remained hidden in previous ansatz-based investigations. Furthermore, we establish the explicit mapping between the intrinsic system parameters and these diverse wave profiles.

The primary objective of this paper is to systematically explore this complete solution space. Specifically, we first carry out a comprehensive qualitative and bifurcation analysis of the phase portraits of system (1.9) under the condition that f possesses three positive roots, and we then identify all possible explicit bounded traveling wave profiles admitted by the PDE (1.1) together with their exact parametric representations.

The remainder of the paper is organized as follows. In Section 2, we analyze the phase portraits and topological classifications of system (1.9). In Sections 3–5, we derive the exact parametric representations for the bounded solutions corresponding to each distinct parameter regime, organized according to the signs of α and μ. Finally, in Section 6, we present concluding remarks and physical discussions.

2. Phase portraits and bifurcation analysis of system (1.9)

In this section, we analyze the dynamics of the ODE system (1.9) to characterize the traveling wave profiles. First, we introduce the rescaling $\xi = (\alpha + 2\mu\rho^2)\zeta$, yielding the following system of equations:

$$\frac{d\rho}{d\zeta} = y(\alpha + 2\mu\rho^2), \quad \frac{dy}{d\zeta} = -\left(2\mu\rho y^2 + b_0\rho + \gamma\rho^3 + \nu\rho^5 + \rho^7\right) = -\rho(2\mu y^2 + f(\rho^2)), \tag{2.1}$$

where $f(s) = b_0 + \gamma s + \nu s^2 + s^3$ and $f'(s) = \gamma + 2\nu s + 3s^2$. If $\Delta = \nu^2 - 3\gamma > 0$, the derivative $f'(s)$ has two real zeros

$$s_{1,2} = \frac{1}{3}(-\nu \mp \sqrt{\Delta}),$$

which are positive if $\nu < 0$ and $\gamma > 0$. For $b_0 < 0$, we have $f(s_1) > 0$ and $f(s_2) < 0$, i.e.,

$$\begin{aligned} &\frac{2}{27}\nu^3 - \frac{1}{3}\gamma\nu + b_0 + \frac{1}{27}(2\nu^2 - 6\gamma)\sqrt{\Delta} > 0, \\ &\frac{2}{27}\nu^3 - \frac{1}{3}\gamma\nu + b_0 - \frac{1}{27}(2\nu^2 - 6\gamma)\sqrt{\Delta} < 0. \end{aligned} \tag{2.2}$$

This implies that $f(s)$ has three simple positive real zeros, and therefore system (2.1) has seven equilibrium points on the ρ-axis: $E_1(\mp\rho_1, 0), E_2(\mp\rho_2, 0), E_3(\mp\rho_3, 0)$, and $O(0,0)$, where $\rho_j = \sqrt{s_j}$ $(j = 1, 2, 3)$. When $\mu\alpha < 0$, we define $\rho_s = \sqrt{-\frac{\alpha}{2\mu}}$. If $Y_s = -\frac{1}{2\mu}f(\rho_s^2) > 0$, then on the straight lines $\rho = \mp\rho_s$, four equilibrium points $S_\mp\left(\mp\rho_s, \mp\sqrt{Y_s}\right)$ exist for system (2.1).

Let $M(\rho_j, 0)$ denote the coefficient matrix of the linearized system at the equilibrium point $E_j(\rho_j, 0)$, and let $J(\cdot,\cdot)$ be the Jacobian determinant. Then,

$$J(0,0) = b_0\alpha, \quad J(\rho_j, 0) = -\rho_j^2(2\gamma + 4\nu\rho_j^2 + 6\rho_j^4).$$

Straightforward computation shows that $J\left(\pm\rho_s, \mp\sqrt{Y_s}\right) = -16\mu^2\rho_s^2 Y_s < 0$, implying that the equilibrium points $S_\mp\left(\mp\rho_s, \mp\sqrt{Y_s}\right)$ are saddle points of system (2.1). For the Hamiltonian $H(\rho, y)$ given by (1.10), we denote $h_0 = H(0,0) = 0$, $h_j = H(\rho_j, 0)$ for $j = 1, 2, 3$, and $h_s = H(\pm\rho_s, \pm\sqrt{Y_s})$.

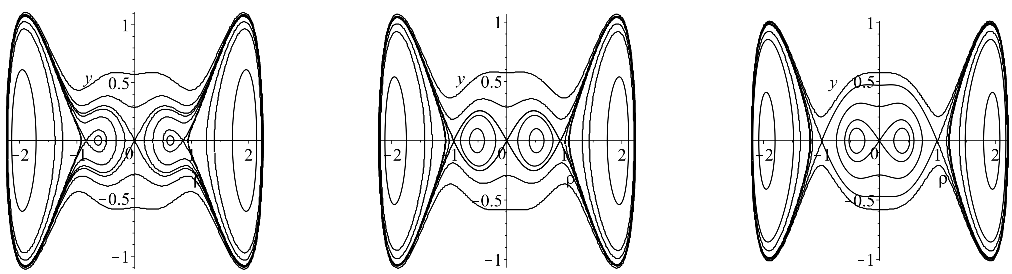

(a) $h_3 < h_1 < h_2 < 0$. (b) $h_3 < h_1 < 0 = h_2$. (c) $h_3 < h_1 < 0 < h_2$.

Figure 1. Phase portraits of system (1.9) when $\alpha > 0, \mu > 0$.

Based on the above analysis, we summarize the dynamical behavior of system (2.1) as follows. Under the assumptions $\nu < 0$, $\gamma > 0$, $b_0 < 0$ and condition (2.2), the function $f(s)$ has three positive simple zeros $0 < s_1 < s_2 < s_3$. Hence $f(\rho^2) = 0$ yields six nonzero roots $\rho = \pm\sqrt{s_j}$ $(j = 1, 2, 3)$, together with $\rho = 0$, giving seven equilibrium points of system (2.1) on the ρ-axis. The equilibrium $O(0,0)$ satisfies $J(0,0) = b_0\alpha > 0$ when $\alpha < 0$, implying that it is a saddle point for $\alpha < 0$ and a center for $\alpha > 0$ (since $b_0 < 0$). Each pair $E_j(\pm\rho_j, 0)$ shares the same Jacobian $J(\rho_j, 0)$. The sign of $J(\rho_j, 0)$ alternates as j increases because $f'(s)$ alternates in sign at its three positive roots; consequently, among E_1, E_2, E_3, one is a center while the other two are saddles, or vice versa.

When $\mu\alpha < 0$, the straight lines $\rho = \pm\rho_s$ are singular. Additional equilibria $S_\mp(\mp\rho_s, \mp\sqrt{Y_s})$ appear provided $Y_s > 0$. Since $J(\pm\rho_s, \mp\sqrt{Y_s}) < 0$, these are always saddle points. The global

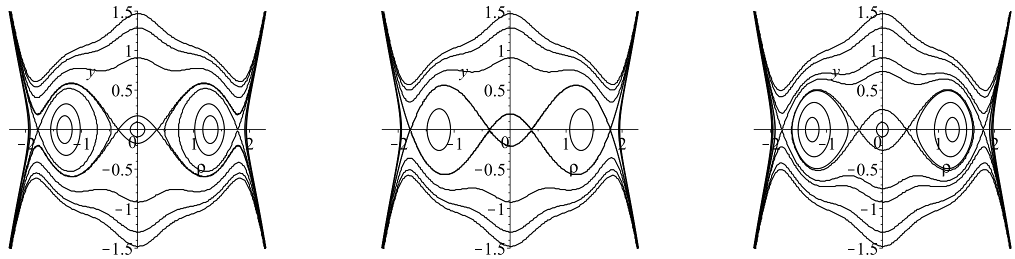

(a) $h_1 < 0 < h_3 < h_2$. (b) $h_1 = h_3 < 0 < h_2$. (c) $h_3 < h_1 < 0 < h_2$.

Figure 2. Phase portraits of system (1.9) when $\alpha < 0, \mu < 0$.

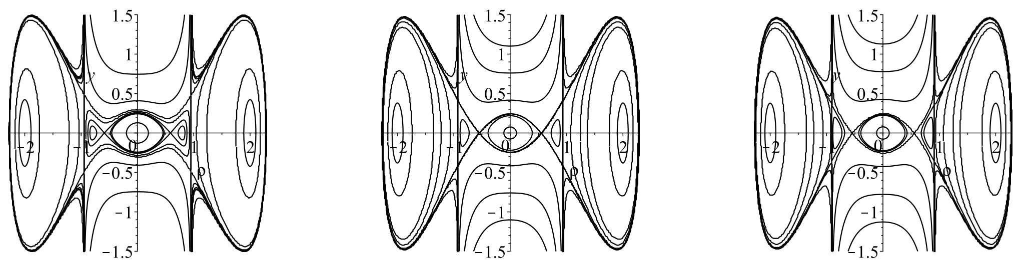

(a) $h_3 < h_s < h_1 < h_2 < 0$. (b) $h_3 < h_s = h_1 < h_2 < 0$. (c) $h_3 < h_1 < h_s < h_2 < 0$.

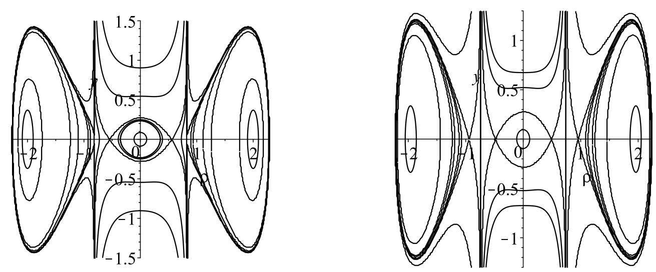

(d) $h_3 < h_1 < h_s = h_2 < 0$. (e) $h_3 < h_1 < 0 < h_2$.

Figure 3. Phase portraits of system (1.9) when $\alpha < 0, \mu > 0$.

phase portraits are governed by the relative ordering of the Hamiltonian values $h_j = H(\rho_j, 0)$ and $h_s = H(\pm\rho_s, \pm\sqrt{Y_s})$, which depend on the parameters α, μ, γ, ν, and b_0.

Specifically, four qualitatively different parameter regimes arise, determined by the signs of α and μ: (i) $\alpha > 0$, $\mu > 0$; (ii) $\alpha < 0$, $\mu < 0$ (both corresponding to $\mu\alpha > 0$, where no singular lines exist); (iii) $\alpha < 0$, $\mu > 0$; and (iv) $\alpha > 0$, $\mu < 0$ (both corresponding to $\mu\alpha < 0$, where singular lines appear). For each regime, the possible relative orderings of $\{h_0, h_1, h_2, h_3\}$ (and h_s when applicable) are determined by the parameters. The corresponding phase portraits are displayed in Figures 1–4. When $\mu\alpha > 0$, system (2.1) is a regular Hamiltonian system without singular lines, and the seven equilibrium points on the ρ-axis determine the topological structure of the phase portraits.

In summary, we have the following classification result.

Theorem 2.1. *Assume the parameters of system* (1.9) *satisfy $\nu < 0$, $\gamma > 0$, and $b_0 = \Omega q - \kappa + \frac{q^2}{4\alpha} < 0$, and that condition* (2.2) *holds. Then, along the ρ-axis of the phase plane (ρ, y), system*

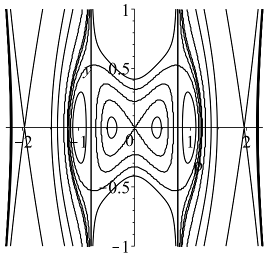

(a) $h_3 < h_1 < 0 < h_s < h_2$.

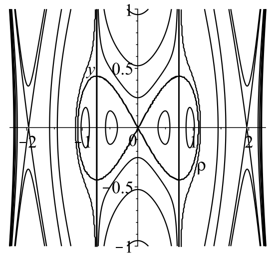

(b) $h_3 < h_1 < 0 = h_s < h_2$.

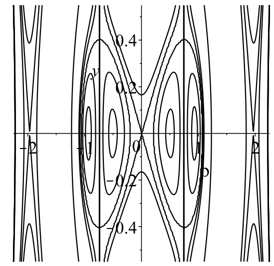

(c) $h_3 < h_1 < h_s < 0 < h_2$.

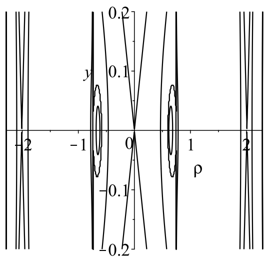

(d) $h_3 < h_1 < h_s = h_2 < 0$.

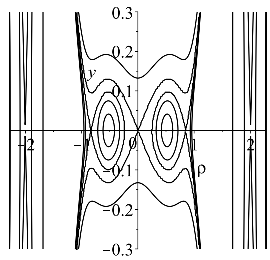

(e) $h_3 < h_1 < 0 = h_2$.

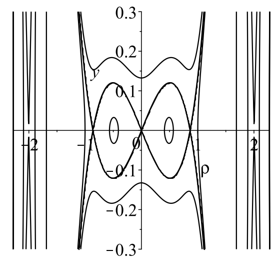

(f) $h_3 < h_1 < h_2 = 0$.

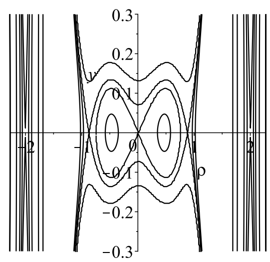

(g) $h_3 < h_1 < 0 < h_2$.

Figure 4. Phase portraits of system (1.9) when $\alpha > 0, \mu < 0$.

(1.9) *possesses seven equilibrium points. Furthermore, the topological classification and global phase portraits of system* (1.9) *are categorized into the configurations shown in Figures 1–4.*

3. Exact parametric representations of bounded solutions for $\mu\alpha > 0$

In this section, we derive exact parametric representations for the bounded orbits shown in Figures 1 and 2. From equation (1.10), we have:

$$y^2 = \frac{h - \left(b_0\rho^2 + \frac{1}{2}\gamma\rho^4 + \frac{1}{3}\nu\rho^6 + \frac{1}{4}\rho^8\right)}{2\mu\rho^2 + \alpha}. \tag{3.1}$$

Using the first equation of system (1.9), we obtain the following integral expression:

$$\xi = \int_{\rho_0}^{\rho} \frac{|2\mu\rho^2 + \alpha| d\rho}{\sqrt{\left|h - \left(b_0\rho^2 + \frac{1}{2}\gamma\rho^4 + \frac{1}{3}\nu\rho^6 + \frac{1}{4}\rho^8\right)\right| |2\mu\rho^2 + \alpha|}}$$

$$= \int_{\phi_0}^{\phi} \frac{|2\mu\phi+\alpha|d\phi}{2\sqrt{\phi\left|h-\left(b_0\phi+\frac{1}{2}\gamma\phi^2+\frac{1}{3}\nu\phi^3+\frac{1}{4}\phi^4\right)\right|\,|2\mu\phi+\alpha|}}, \tag{3.2}$$

where $\phi=\rho^2$. For the orbits shown in Figures 1–4, the integral on the right-hand side of (3.2) can be evaluated explicitly in terms of elliptic and elementary functions.

3.1. The case $\alpha>0, \mu>0$.

(i) When $h_3<h_1<h_2<0$ in Figure 1(a), the level curves defined by $H(\rho,y)=0$ and $H(\rho,y)=h_2$ are shown in Figures 5(a) and (b).

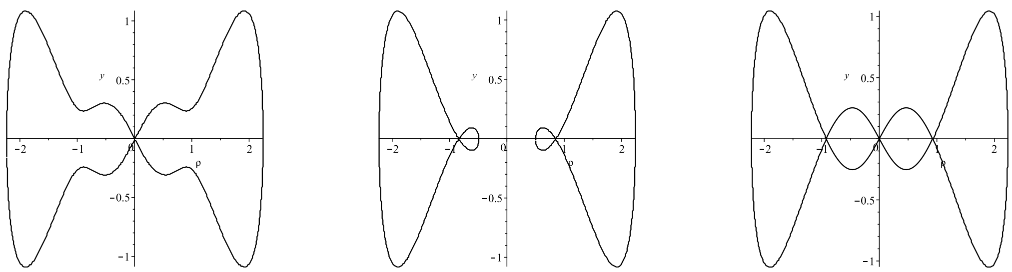

(a) $h=h_0=0$. (b) $h=h_2$. (c) $h=0=h_2$.

Figure 5. Level curves of system (1.9) defined by $H(\rho,y)=h$ when $\alpha>0,\mu>0$.

(1) Consider the double homoclinic orbits defined by $H(\rho,y)=0$ in Figure 5(a), which enclose three equilibrium points. For the left orbit, formula (3.2) can be rewritten as

$$\sqrt{2\mu}\xi = \int_{-\phi_M}^{\phi} \frac{(2\mu\phi+\alpha)d\phi}{\phi\sqrt{(\phi-\phi_M)\left(\phi+\frac{\alpha}{2\mu}\right)\left[(\phi-b_1)^2+a_1^2\right]}}.$$

Thus, we obtain the following two homoclinic solutions:

$$\rho(\chi)=\mp\left|\frac{\frac{\alpha A_1}{2\mu}-\phi_M B_1-\left(\phi_M B_1+\frac{\alpha A_1}{2\mu}\right)\mathrm{cn}(\chi,k)}{(A_1-B_1)-(A_1+B_1)\mathrm{cn}(\chi,k)}\right|^{\frac{1}{2}}, \quad \chi\in(-\chi_{01},\chi_{01}),$$
$$\xi(\chi)=\frac{1}{\sqrt{2\mu}}\left[\frac{2\mu}{\sqrt{A_1B_1}}\chi+\alpha\int_{-\phi_M}^{\phi}\frac{d\phi}{\phi\sqrt{(\phi-\phi_M)\left(\phi+\frac{\alpha}{2\mu}\right)\left[(\phi-b_1)^2+a_1^2\right]}}\right], \tag{3.3}$$

where $A_1^2=(\phi_M-b_1)^2+a_1^2$, $B_1^2=\left(\frac{\alpha}{2\mu}-b_1\right)^2+a_1^2$, $k^2=\frac{(A_1+B_1)^2-\left(\phi_M-\frac{\alpha}{2\mu}\right)^2}{4A_1B_1}$, $\chi_{01}=\mathrm{cn}^{-1}\left(\frac{\frac{\alpha A_1}{2\mu}-\phi_M B_1}{\frac{\alpha A_1}{2\mu}+\phi_M B_1}\right)$, and $\mathrm{cn}(\cdot,k)$ is the Jacobi elliptic function (see [3]).

For the two double homoclinic orbits defined by $H(\rho,y)=h_2$, illustrated in Figure 5(b), where each homoclinic loop encloses one equilibrium point, the integral (3.2) gives

$$\sqrt{2\mu}\xi = \int_{\phi}^{\phi_M} \frac{(2\mu\phi+\alpha)d\phi}{(\phi-\phi_2)\sqrt{(\phi_M-\phi)(\phi-\phi_m)\phi\left(\phi+\frac{\alpha}{2\mu}\right)}}$$

and

$$\sqrt{2\mu}\xi = \int_{\phi_m}^{\phi} \frac{(2\mu\phi + \alpha)d\phi}{(\phi_2 - \phi)\sqrt{(\phi_M - \phi)(\phi - \phi_m)\phi\left(\phi + \frac{\alpha}{2\mu}\right)}}.$$

Hence, we obtain the following four homoclinic solutions:

$$\begin{aligned}
\rho(\chi) &= \mp\left(-\frac{\alpha}{2\mu} + \frac{\phi_M + \frac{\alpha}{2\mu}}{1 - \hat{\alpha}_1^2 \mathrm{sn}^2(\chi, k)}\right)^{\frac{1}{2}}, \quad \chi \in (-\chi_{02}, \chi_{02}), \\
\xi(\chi) &= \frac{2}{\sqrt{(2\mu\phi_m + \alpha)\phi_M}}\left[\left(\frac{2\mu\phi_M}{\phi_M - \phi_m}\right)\chi \right. \\
&\quad \left. + \left(\frac{\alpha + 2\mu\phi_2}{\phi_m - \phi_2} - \frac{2\mu\phi_m}{\phi_M - \phi_m}\right)\Pi\left(\arcsin\left(\mathrm{sn}(\chi, k)\right), \tilde{\alpha}_1^2, k\right)\right],
\end{aligned} \tag{3.4}$$

where $k^2 = \frac{(\phi_M - \phi_m)\alpha}{\phi_M(2\mu\phi_m + \alpha)}$, $\hat{\alpha}_1^2 = \frac{\phi_m - \phi_M}{\phi_m + \frac{\alpha}{2\mu}}$, $\tilde{\alpha}_1^2 = \frac{(2\mu\phi_2 + \alpha)(\phi_M - \phi_m)}{(\phi_M - \phi_2)(2\mu\phi_m + \alpha)}$, $\chi_{02} = \mathrm{sn}^{-1}\sqrt{\frac{(\phi_2 - \phi_m)(2\mu\phi_m + \alpha)}{(\phi_M - \phi_m)(2\mu\phi_2 + \alpha)}}$, $\mathrm{sn}(\cdot, k)$ is the Jacobi elliptic function, and $\Pi(\cdot, \tilde{\alpha}_1^2, k)$ is the incomplete elliptic integral of the third kind. Furthermore,

$$\begin{aligned}
\rho(\chi) &= \mp\left(\frac{\phi_m}{1 - \hat{\alpha}_2^2 \mathrm{sn}^2(\chi, k)}\right)^{\frac{1}{2}}, \quad \chi \in (-\chi_{03}, \chi_{03}), \\
\xi(\chi) &= \frac{2}{\sqrt{(2\mu\phi_m + \alpha)\phi_M}}\left[\left(\frac{\alpha}{\phi_2} - \mu\right)\chi + \left(\frac{\phi_M(\alpha + 2\mu\phi_2)}{(\phi_2 - \phi_m)\phi_2}\right)\Pi\left(\arcsin\left(\mathrm{sn}(\chi, k)\right), \tilde{\alpha}_2^2, k\right)\right],
\end{aligned} \tag{3.5}$$

where $k^2 = \frac{\alpha\tilde{\alpha}_1^2}{2\mu\phi_m + \alpha}$, $\hat{\alpha}_2^2 = 1 - \frac{\phi_m}{\phi_M}$, $\tilde{\alpha}_2^2 = \frac{\phi_2(\phi_M - \phi_m)}{(\phi_2 - \phi_m)\phi_M}$, and $\chi_{03} = \mathrm{sn}^{-1}\sqrt{\frac{\phi_M(\phi_2 - \phi_m)}{(\phi_M - \phi_m)\phi_2}}$.

(ii) When $h_3 < h_1 < h_2 = 0$, the level curves defined by $H(\rho, y) = 0 = h_2$ are illustrated in Figure 5(c).

(1) For the four heteroclinic orbits defined by $H(\rho, y) = 0$, enclosing the equilibrium points $E_1(\mp\rho_1, 0)$, equation (3.2) becomes

$$\sqrt{2\mu}\xi = \int_{\phi_1}^{\phi} \frac{(2\mu\phi + \alpha)d\phi}{\phi(\phi_2 - \phi)\sqrt{(\phi_M - \phi)\left(\phi + \frac{\alpha}{2\mu}\right)}} = \int_{\phi_1}^{\phi} \frac{(2\mu\phi + \alpha)d\phi}{\phi(\phi_2 - \phi)\sqrt{X(\phi)}},$$

with $X(\phi) = (\phi_M - \phi)(\phi + \frac{\alpha}{2\mu})$. The exact parametric representations of the four kink wave solutions are:

$$\begin{aligned}
\rho(\chi) &= \mp\left(\frac{\frac{\alpha}{\mu}\phi_M}{P_0 \cosh_{q_0}\left(\sqrt{\frac{\alpha\phi_M}{2\mu}}\chi\right) - (\phi_M - \frac{\alpha}{2\mu})}\right)^{\frac{1}{2}}, \\
\xi(\chi) &= \pm\frac{1}{\sqrt{2\mu}}\left[2\mu\chi + (2\mu\phi_2 + \alpha)\int_{\phi_1}^{\phi} \frac{d\phi}{\phi(\phi_2 - \phi)\sqrt{X(\phi)}}\right],
\end{aligned} \tag{3.6}$$

where $P_0 = \frac{1}{\phi_1}\left(2\sqrt{\frac{\alpha\phi_M}{2\mu}X(\phi_1)} + (\phi_M - \frac{\alpha}{2\mu})\phi_1 + \frac{\alpha\phi_M}{\mu}\right)$, $q_0 = \frac{(\phi_M + \frac{\alpha}{2\mu})^2}{P_0^2}$, $\cosh_{q_0}(a\chi)$ is the Arai

q-deformed function [1,2] defined by $\cosh_q(\phi) = \frac{1}{2}(e^{\phi} + qe^{-\phi})$, and

$$\int \frac{d\phi}{\phi(\phi_2-\phi)\sqrt{X(\phi)}} = \frac{1}{\phi_2\sqrt{X(\phi_2)}} \ln\left|\frac{2\sqrt{X(\phi_2)X(\phi)} - (\phi_M - 2\phi_2 - \frac{\alpha}{2\mu})(\phi_2-\phi) + 2X(\phi_2)}{\phi_2-\phi}\right|$$
$$- \frac{1}{\phi_2\sqrt{\frac{\alpha\phi_M}{2\mu}}} \ln\left|\frac{2\sqrt{\frac{\alpha\phi_M}{2\mu}X(\phi)} + (\phi_M - \frac{\alpha}{2\mu})\phi + \frac{\alpha\phi_M}{\mu}}{\phi}\right|.$$

(2) For the two homoclinic orbits defined by $H(\rho, y) = 0$ enclosing the two equilibrium points $E_3(\mp\rho_3, 0)$ in Figure 5(c), we have

$$\sqrt{2\mu}\xi = \int_{\phi}^{\phi_M} \frac{(2\mu\phi+\alpha)d\phi}{\phi(\phi-\phi_2)\sqrt{(\phi_M-\phi)\left(\phi+\frac{\alpha}{2\mu}\right)}},$$

yielding the two solitary wave solutions:

$$\rho(\chi) = \mp\left(\phi_2 + \frac{2(\phi_M-\phi_2)\left(\phi_2+\frac{\alpha}{2\mu}\right)}{(\phi_M+\frac{\alpha}{2\mu})\cosh\left(\sqrt{(\phi_M-\phi_2)\left(\phi_2+\frac{\alpha}{2\mu}\right)}\chi\right) - (\phi_M-2\phi_2-\frac{\alpha}{2\mu})}\right)^{\frac{1}{2}},$$
$$\xi(\chi) = \frac{1}{\sqrt{2\mu}}\left[2\mu\chi + \alpha\int_{\phi}^{\phi_M}\frac{d\phi}{\phi(\phi_2-\phi)\sqrt{X(\phi)}}\right]. \tag{3.7}$$

(iii) When $h_3 < h_1 < 0 < h_2$, the level curves defined by $H(\rho, y) = 0$ and $H(\rho, y) = h_2$ are shown in Figure 6.

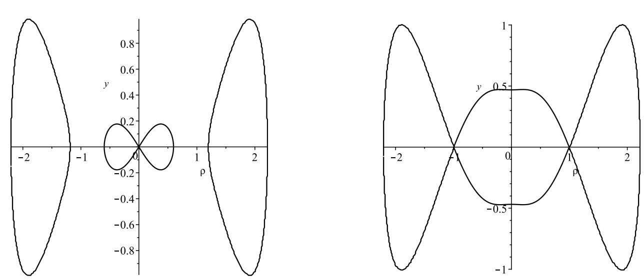

(a) $h = h_0 = 0$. (b) $h = h_2$.

Figure 6. Level curves of system (1.9) defined by $H(\rho, y) = h$ when $\alpha > 0, \mu > 0$.

(1) For the double homoclinic orbits defined by $H(\rho, y) = 0$ in Figure 6(a), each branch enclosing an equilibrium point, expression (3.2) gives

$$\sqrt{2\mu}\xi = \int_{\phi}^{\phi_M} \frac{(2\mu\phi+\alpha)d\phi}{\phi\sqrt{(\phi_a-\phi)(\phi-\phi_b)(\phi_M-\phi)\left(\phi+\frac{\alpha}{2\mu}\right)}},$$

yielding two solitary wave solutions:

$$\begin{aligned}\rho(\chi) &= \mp\left(\phi_b - \frac{\phi_b-\phi_M}{1-\hat{\alpha}_3^2\mathrm{sn}^2(\chi,k)}\right)^{\frac{1}{2}}, \quad \chi\in(-\chi_{04},\chi_{04}),\\ \xi(\chi) &= \frac{2}{\sqrt{(2\mu\phi_b+\alpha)(\phi_b-\phi_M)}}\left[\left(\frac{\alpha}{\phi_b}+2\mu\right)\chi + \left(\frac{\alpha(\phi_b-\phi_M)}{\phi_b\phi_M}\right)\Pi\left(\arcsin\left(\mathrm{sn}(\chi,k)\right),\tilde{\alpha}_3^2,k\right)\right],\end{aligned} \tag{3.8}$$

where $k^2=\frac{\hat{\alpha}_3^2(\phi_a-\phi_b)}{\phi_a-\phi_M}$, $\hat{\alpha}_3^2=\frac{\phi_M+\frac{\alpha}{2\mu}}{\phi_b+\frac{\alpha}{2\mu}}$, $\tilde{\alpha}_3^2=\frac{\phi_b\hat{\alpha}_3^2}{\phi_M}$, and $\chi_{04}=\mathrm{sn}^{-1}\sqrt{\frac{\phi_M(\phi_b+\frac{\alpha}{2\mu})}{(\phi_M+\frac{\alpha}{2\mu})\phi_b}}$.

(2) For the two periodic orbits defined by $H(\rho,y)=0$, each enclosing one of the equilibrium points $E_3(\mp\rho_3,0)$ in Figure 6(a), we have:

$$\begin{aligned}\rho(\chi) &= \mp\left(\phi_M + \frac{\phi_b-\phi_M}{1-\hat{\alpha}_4^2\mathrm{sn}^2(\chi,k)}\right)^{\frac{1}{2}},\\ \xi(\chi) &= \frac{2}{\sqrt{(2\mu\phi_b+\alpha)(\phi_b-\phi_M)}}\left[\left(\frac{\phi_b}{\phi_M}+2\mu\right)\chi - \left(\frac{\alpha(\phi_b-\phi_M)}{\phi_b\phi_M}\right)\Pi\left(\arcsin\left(\mathrm{sn}(\chi,k)\right),\tilde{\alpha}_4^2,k\right)\right],\end{aligned} \tag{3.9}$$

where $k^2=\frac{\hat{\alpha}_4^2(\phi_M+\frac{\alpha}{2\mu})}{\phi_b+\frac{\alpha}{2\mu}}$, $\hat{\alpha}_4^2=\frac{\phi_a-\phi_b}{\phi_a-\phi_M}$, and $\tilde{\alpha}_4^2=\frac{\phi_M\hat{\alpha}_4^2}{\phi_b}$.

(3) For the two heteroclinic loops defined by $H(\rho,y)=h_2$, enclosing the origin in Figure 6(b), we have the kink and anti-kink wave solutions:

$$\begin{aligned}\rho(\chi) &= \left(-\phi_c + \frac{\phi_c}{1-\hat{\alpha}_5^2\mathrm{sn}^2(\chi,k)}\right)^{\frac{1}{2}}, \quad \chi\in(-\chi_{05},\chi_{05}),\\ \xi(\chi) &= \mp\frac{2}{\sqrt{(\phi_M+\phi_c)\alpha}}\left[\left(\frac{2\mu\phi_2+\alpha}{\phi_2+\phi_c}-2\mu\right)\chi + \left(\frac{(2\mu\phi_2+\alpha)\phi_2}{\phi_2(\phi_2+\phi_c)}\right)\Pi\left(\arcsin\left(\mathrm{sn}(\chi,k)\right),\tilde{\alpha}_5^2,k\right)\right],\end{aligned} \tag{3.10}$$

where $k^2=\frac{\hat{\alpha}_5^2(\frac{\alpha}{2\mu}-\phi_c)}{\frac{\alpha}{2\mu}}$, $\hat{\alpha}_5^2=\frac{\phi_M}{\phi_M+\phi_c}$, $\tilde{\alpha}_5^2=\frac{(\phi_2+\phi_c)\hat{\alpha}_5^2}{\phi_2}$, and $\chi_{05}=\mathrm{sn}^{-1}\sqrt{\frac{\phi_2(\phi_M+\phi_c)}{(\phi_2+\phi_c)\phi_M}}$.

(4) For the two homoclinic orbits defined by $H(\rho,y)=h_2$ in Figure 6(b), we have the two solitary wave solutions:

$$\begin{aligned}\rho(\chi) &= \mp\left(-\frac{\alpha}{2\mu} + \frac{\phi_M+\frac{\alpha}{2\mu}}{1-\hat{\alpha}_6^2\mathrm{sn}^2(\chi,k)}\right)^{\frac{1}{2}}, \quad \chi\in(-\chi_{06},\chi_{06}),\\ \xi(\chi) &= \frac{2}{\sqrt{(\phi_M+\phi_c)\alpha}}\left[4\mu\chi + \left(\frac{2\mu(2\phi_2-\phi_M+\frac{\alpha}{2\mu})}{\phi_M-\phi_2}\right)\Pi\left(\arcsin\left(\mathrm{sn}(\chi,k)\right),\tilde{\alpha}_6^2,k\right)\right],\end{aligned} \tag{3.11}$$

where $k^2=\frac{-\hat{\alpha}_6^2(\frac{\alpha}{2\mu}-\phi_c)}{\phi_M+\phi_c}$, $\hat{\alpha}_6^2=\frac{-2\mu\phi_M}{\alpha}$, $\tilde{\alpha}_6^2=\frac{-(\phi_2+\frac{\alpha}{2\mu})\hat{\alpha}_6^2}{\phi_M-\phi_2}$, and $\chi_{06}=\mathrm{sn}^{-1}\sqrt{\frac{\alpha(\phi_M-\phi_2)}{(2\mu\phi_2+\alpha)\phi_M}}$.

3.2. The case $\alpha<0,\mu<0$.

(i) When $h_1<0<h_3<h_2$, the level curves defined by $H(\rho,y)=h_1$ and $H(\rho,y)=h_3$ are shown in Figures 7(a) and (b).

(1) For the heteroclinic loop in Figure 7(a) enclosing the origin $O(0,0)$, we obtain the kink

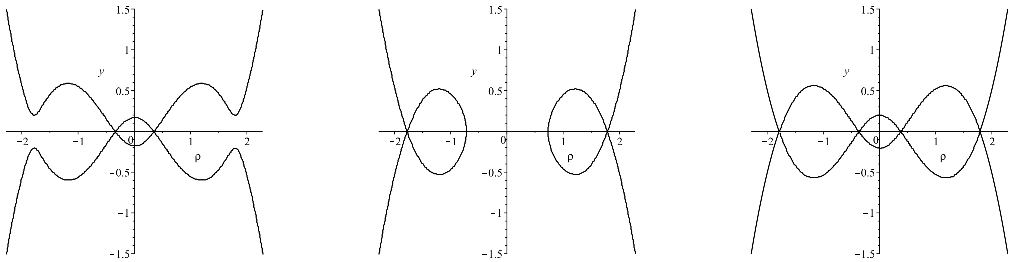

(a) $h=h_1$. (b) $h=h_3$. (c) $h=h_1=h_3$.

Figure 7. Level curves of system (1.9) defined by $H(\rho,y)=h$ when $\alpha<0,\mu<0$.

and anti-kink wave solutions:

$$\rho(\chi)=\mp\left|\frac{\frac{\alpha A_2}{2\mu}(1-\mathrm{cn}(\chi,k))}{(A_2-B_2)-(A_2+B_2)\mathrm{cn}(\chi,k)}\right|^{\frac{1}{2}},\quad \chi\in(-\chi_{07},\chi_{07}),$$

$$\xi(\chi)=\mp\frac{1}{\sqrt{2|\mu|}}\left[-\frac{2|\mu|}{\sqrt{A_2B_2}}\chi+(2|\mu|\phi_1+|\alpha|)\int_0^\phi\frac{d\phi}{(\phi_1-\phi)\sqrt{\phi\left(\phi+\frac{\alpha}{2\mu}\right)[(\phi-b_2)^2+a_2^2]}}\right],\tag{3.12}$$

where $A_2^2=b_2^2+a_2^2$, $B_2^2=\left(\frac{\alpha}{2\mu}-b_2\right)^2+a_2^2$, $k^2=\frac{(A_2+B_2)^2-\left(\frac{\alpha}{2\mu}\right)^2}{4A_2B_2}$, and $\chi_{07}=\mathrm{cn}^{-1}\left(\frac{2\mu\phi_1(A_2-B_2)-\alpha A_2}{2\mu\phi_1(A_2+B_2)-\alpha A_2}\right)$.

(2) For the two homoclinic orbits defined by $H(\rho,y)=h_3$ in Figure 7(b), enclosing the two equilibria $E_2(\mp\rho_2,0)$, we have:

$$\begin{aligned}\rho(\chi)&=\mp\left(\frac{\phi_m}{1-\hat{\alpha}_7^2\mathrm{sn}^2(\chi,k)}\right)^{\frac{1}{2}},\quad \chi\in(-\chi_{08},\chi_{08}),\\ \xi(\chi)&=\frac{2}{\sqrt{(\phi_M+\phi_c)|\alpha|}}\left[\left(-2|\mu|+\frac{2|\mu|\phi_3+|\alpha|}{\phi_3}\right)\chi\right.\\ &\quad\left.+\left(\frac{(2|\mu|\phi_3+|\alpha|)\phi_M}{(\phi_3-\phi_m)\phi_3}\right)\Pi\left(\arcsin\left(\mathrm{sn}(\chi,k)\right),\tilde{\alpha}_7^2,k\right)\right],\end{aligned}\tag{3.13}$$

where $k^2=\frac{\hat{\alpha}_7^2\phi_c}{\phi_M+\phi_c}$, $\hat{\alpha}_7^2=\frac{2|\mu|\phi_m+|\alpha|}{|\alpha|}$, $\tilde{\alpha}_7^2=\frac{-(\phi_2+\frac{\alpha}{2\mu})\hat{\alpha}_6^2}{\phi_M-\phi_2}$, and $\chi_{08}=\mathrm{sn}^{-1}\sqrt{\frac{\alpha(\phi_3-\phi_m)}{(2|\mu|\phi_m+|\alpha|)\phi_3}}$.

(ii) When $h_3=h_1<h_2<0$, the level curve defined by $H(\rho,y)=h_1=h_3$ is displayed in Figure 7(c).

(1) For the heteroclinic loop enclosing the origin, we obtain the kink wave solutions:

$$\begin{aligned}\rho(\chi)&=\pm\left(\phi_1-\frac{2\phi_1(2|\mu|\phi_1+|\alpha|)}{|\alpha|\cosh\left(\sqrt{\phi_1(\phi_1+\frac{\alpha}{2\mu})}\chi\right)+(4|\mu|\phi_1+|\alpha|)}\right)^{\frac{1}{2}},\\ \xi(\chi)&=\pm\frac{1}{\sqrt{2|\mu|}}\left[-2\mu\chi+(2|\mu|\phi_3+|\alpha|)\int_0^\phi\frac{d\phi}{(\phi_1-\phi)(\phi_3-\phi)\sqrt{X_1(\phi)}}\right],\end{aligned}\tag{3.14}$$

where

$$\int \frac{d\phi}{(\phi_1-\phi)(\phi_3-\phi)\sqrt{X_1(\phi)}}$$
$$=\frac{1}{(\phi_3-\phi_1)\sqrt{X_1(\phi_1)}}\ln\left|\frac{2\sqrt{X_1(\phi_1)X_1(\phi)}-(2\phi_1+\frac{\alpha}{2\mu})(\phi_1-\phi)+2X_1(\phi_1)}{\phi_1-\phi}\right|$$
$$-\frac{1}{(\phi_3-\phi_1)\sqrt{X_1(\phi_3)}}\ln\left|\frac{2\sqrt{X_1(\phi_3)X_1(\phi)}-(2\phi_3+\frac{\alpha}{2\mu})(\phi_3-\phi)+2X_1(\phi_3)}{\phi_3-\phi}\right|.$$

(2) For the heteroclinic loops defined by $H(\rho,y)=h_3=h_1$ in Figure 7(c) enclosing the two equilibria $E_2(\mp\rho_2,0)$, we obtain:

$$\begin{aligned}\rho(\chi)&=\pm\left(\phi_3+\frac{2(\phi_3+\frac{\alpha}{2\mu})\phi_3}{P_1\cosh_{q_1}\left(\sqrt{(\phi_3+\frac{\alpha}{2\mu})\phi_3}\chi\right)+(2\phi_3+\frac{\alpha}{2\mu})}\right)^{\frac{1}{2}},\\ \xi(\chi)&=\pm\frac{1}{\sqrt{2|\mu|}}\left[2|\mu|\chi+(2|\mu|\phi_1+|\alpha|)\int_{\phi_2}^{\phi}\frac{d\phi}{(\phi-\phi_1)(\phi_3-\phi)\sqrt{X_1(\phi)}}\right],\end{aligned}\tag{3.15}$$

where $P_1=\frac{1}{\phi_2}\left(2\sqrt{(\phi_3+\frac{\alpha}{2\mu})\phi_3X_1(\phi_2)}-(2\phi_3+\frac{\alpha}{2\mu})\phi_2+2(\phi_3+\frac{\alpha}{2\mu})\phi_3\right)$ and $q_1=\frac{\alpha^2}{4\mu^2P_1^2}$.

(iii) When $h_3<h_1<0<h_2$, the level curves defined by $H(\rho,y)=h_1$ and $H(\rho,y)=h_3$ are shown in Figures 8(a) and (b).

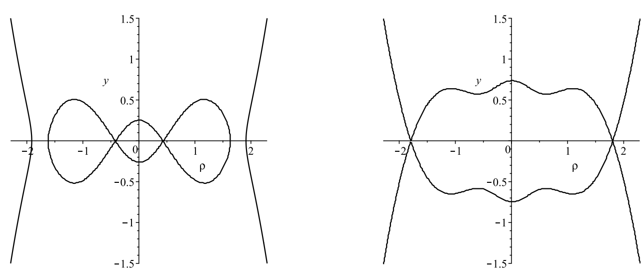

(a) $h=h_1$. (b) $h=h_3$.

Figure 8. Level curves of system (1.9) defined by $H(\rho,y)=h$ when $\alpha<0,\mu<0$.

(1) For the heteroclinic loop defined by $H(\rho,y)=h_1$ enclosing the origin $O(0,0)$ in Figure 8(a), we obtain:

$$\begin{aligned}\rho(\chi)&=\mp\left(-\frac{\alpha}{2\mu}+\frac{\frac{\alpha}{2\mu}}{1-\hat{\alpha}_8^2\mathrm{sn}^2(\chi,k)}\right)^{\frac{1}{2}},\quad \chi\in(-\chi_{09},\chi_{09}),\\ \xi(\chi)&=\frac{2}{\sqrt{\phi_L(2\mu\phi_M+|\alpha|)}}\left[\frac{|\alpha|}{\phi_1}\Pi\left(\arcsin\left(\mathrm{sn}(\chi,k)\right),\tilde{\alpha}_8^2,k\right)\right],\end{aligned}\tag{3.16}$$

where $k^2=\hat{\alpha}_8^2(1+\frac{\alpha}{2\mu\phi_L})$, $\hat{\alpha}_8^2=\frac{\phi_M}{\phi_M+\frac{\alpha}{2\mu}}$, $\tilde{\alpha}_8^2=(1+\frac{\alpha}{2\mu\phi_1})\hat{\alpha}_8^2$, and $\chi_{09}=\mathrm{sn}^{-1}\sqrt{\frac{\phi_1(\phi_M+\frac{\alpha}{2\mu})}{(\phi_1+\frac{\alpha}{2\mu})\phi_M}}$.

(2) For the two homoclinic orbits defined by $H(\rho, y) = h_1$ in Figure 8(a), enclosing $E_2(\mp\rho_2, 0)$, we obtain:

$$\begin{aligned} \rho(\chi) &= \mp\left(\phi_L - \frac{\phi_L - \phi_M}{1 - \hat{\alpha}_9^2 \mathrm{sn}^2(\chi, k)}\right)^{\frac{1}{2}}, \quad \chi \in (-\chi_{010}, \chi_{010}), \\ \xi(\chi) &= \frac{2}{\sqrt{\phi_L(2\mu\phi_M + |\alpha|)}}\left[\left(2|\mu| + \frac{2|\mu|\phi_1 + |\alpha|}{\phi_L - \phi_1}\right)\chi \right. \\ &\quad \left. + \left(\frac{(2\mu\phi_M + |\alpha|)(\phi_L - \phi_M)}{(\phi_M - \phi_1)(\phi_L - \phi_1)}\right)\Pi\left(\arcsin\left(\mathrm{sn}(\chi, k)\right), \tilde{\alpha}_9^2, k\right)\right], \end{aligned} \tag{3.17}$$

where $k^2 = \frac{\hat{\alpha}_9^2(\phi_L + \frac{\alpha}{2\mu})}{\phi_M - \frac{\alpha}{2\mu}}$, $\hat{\alpha}_9^2 = \frac{\phi_M}{\phi_L}$, $\tilde{\alpha}_9^2 = \frac{\hat{\alpha}_9^2(\phi_L - \phi_1)}{\phi_M - \phi_1}$, and $\chi_{010} = \mathrm{sn}^{-1}\sqrt{\frac{\phi_L(\phi_M - \phi_1)}{(\phi_L - \phi_1)\phi_M}}$.

(3) For the heteroclinic loop defined by $H(\rho, y) = h_3$ in Figure 8(b), enclosing five equilibria, we obtain:

$$\begin{aligned} \rho(\chi) &= \mp\left|\frac{\frac{\alpha A_3}{2\mu}(1 - \mathrm{cn}(\chi, k))}{(A_3 - B_3) - (A_3 + B_3)\mathrm{cn}(\chi, k)}\right|^{\frac{1}{2}}, \quad \chi \in (-\chi_{011}, \chi_{011}), \\ \xi(\chi) &= \mp\frac{1}{\sqrt{2|\mu|}}\left[-\frac{2|\mu|}{\sqrt{A_3 B_3}}\chi + (2|\mu|\phi_3 + |\alpha|)\int_0^{\phi}\frac{d\phi}{(\phi_3 - \phi)\sqrt{\phi\left(\phi + \frac{\alpha}{2\mu}\right)[(\phi - b_3)^2 + a_3^2]}}\right], \end{aligned} \tag{3.18}$$

where $A_3^2 = b_3^2 + a_3^2$, $B_3^2 = \left(\frac{\alpha}{2\mu} - b_3\right)^2 + a_3^2$, $k^2 = \frac{(A_3 + B_3)^2 - \left(\frac{\alpha}{2\mu}\right)^2}{4A_3B_3}$, and $\chi_{011} = \mathrm{cn}^{-1}\left(\frac{2\mu\phi_3(A_3 - B_3) - \alpha A_3}{2\mu\phi_3(A_3 + B_3) - \alpha A_3}\right)$.

In summary, the following theorem is established.

Theorem 3.1. *Assume that $\alpha\mu > 0$ and the conditions of Theorem 2.1 hold. Then, system* (1.9) *admits the exact explicit parametric representations $(\rho(\chi), \xi(\chi))$:*

(i) *Exact explicit homoclinic solutions given by equations* (3.3), (3.4), (3.5), (3.7), (3.8), (3.11), (3.13), *and* (3.17).

(ii) *Exact explicit heteroclinic solutions given by equations* (3.6), (3.10), (3.12), (3.14), (3.15), (3.16), *and* (3.18).

(iii) *Exact explicit periodic solutions given by equation* (3.9).

4. Exact parametric representations of bounded solutions for $\alpha < 0, \mu > 0$

In this section, we derive the precise parametric representations for the bounded traveling waves corresponding to Figure 3.

4.1. The case $h_3 < h_s < h_1 < h_2 < 0$ in Figure 3(a).

The level curves defined by $H(\rho, y) = h_s$ and $H(\rho, y) = h_1$ are highlighted in Figures 9(a) and (b).

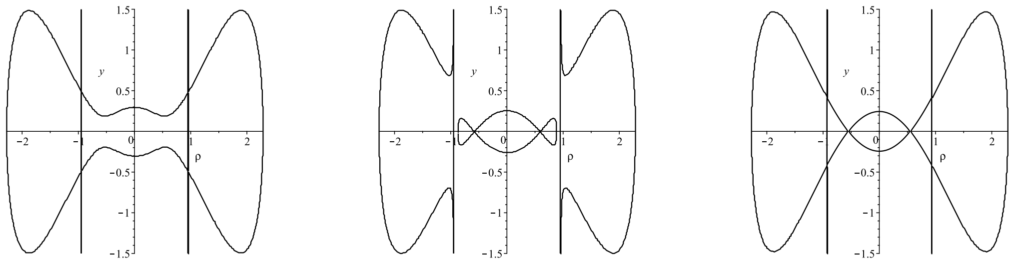

(a) $h = h_s$. (b) $h = h_1$. (c) $h = h_1 = h_s$.

Figure 9. Level curves of system (1.9) defined by $H(\rho, y) = h$ when $\alpha < 0, \mu > 0$.

(i) For the closed orbit defined by $H(\rho, y) = h_s$ in Figure 9(a), we obtain the periodic wave solution:

$$\rho(\xi) = \mp \left| \frac{\phi_M B_4(1 - \mathrm{cn}(\sqrt{A_4 B_4}\xi, k))}{(A_4 + B_4) + (A_4 - B_4)\mathrm{cn}(\sqrt{A_4 B_4}\xi, k)} \right|^{\frac{1}{2}}, \tag{4.1}$$

where $A_4^2 = (\phi_M - b_4)^2 + a_4^2$, $B_4^2 = b_4^2 + a_4^2$, and $k^2 = \frac{\phi_M^2 - (A_4 - B_4)^2}{4 A_4 B_4}$.

When $\xi = \xi_{s0} = \frac{1}{\sqrt{A_4 B_4}} \mathrm{cn}^{-1} \left(\frac{\phi_M B_4 - \frac{|\alpha|}{2\mu}(A_4 + B_4)}{\frac{|\alpha|}{2\mu}(A_4 - B_4) - B_4 \phi_M} \right)$, we have $\rho(\xi_{s0}) = \rho_s$. Thus,

$$\rho(\xi) = \mp \left| \frac{\phi_M B_4(1 - \mathrm{cn}(\sqrt{A_4 B_4}\xi, k))}{(A_4 + B_4) + (A_4 - B_4)\mathrm{cn}(\sqrt{A_4 B_4}\xi, k)} \right|^{\frac{1}{2}}, \quad \xi \in (-\xi_{s0}, 0) \cup (0, \xi_{s0}) \tag{4.2}$$

gives rise to a sawtooth wave solution (see Figure 10(b)). In addition,

$$\rho(\xi) = \mp \left| \frac{\phi_M B_4(1 - \mathrm{cn}(\sqrt{A_4 B_4}\xi, k))}{(A_4 + B_4) + (A_4 - B_4)\mathrm{cn}(\sqrt{A_4 B_4}\xi, k)} \right|^{\frac{1}{2}}, \quad \xi \in (-\xi_{s0}, \xi_{s0}) \tag{4.3}$$

gives rise to two periodic peakon wave solutions (see Figure 10(a)).

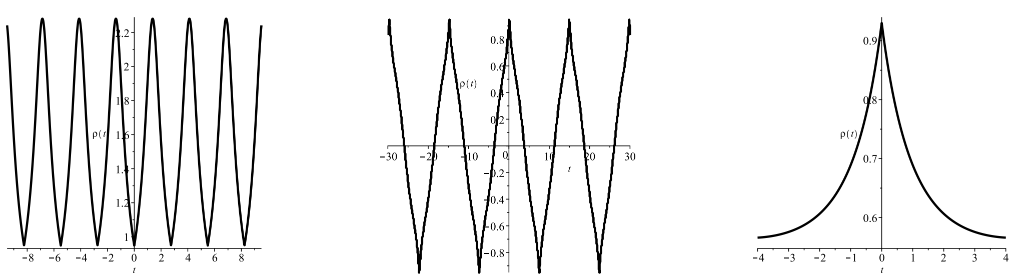

(a) Periodic peakon. (b) Sawtooth wave. (c) Peakon.

Figure 10. Wave profiles of system (1.9) when $\alpha < 0, \mu > 0$.

(ii) Corresponding to the heteroclinic loop enclosing the origin in Figure 9(b), we obtain a pair of kink and anti-kink wave solutions:

$$\rho(\chi) = \mp\left(\frac{-\phi_L\hat{\alpha}_{10}^2\mathrm{sn}^2(\chi,k)}{1-\hat{\alpha}_{10}^2\mathrm{sn}^2(\chi,k)}\right)^{\frac{1}{2}}, \quad \chi\in(-\chi_{012},\chi_{012}),$$

$$\xi(\chi) = \mp\frac{2}{\sqrt{(\phi_L-\phi_M)|\alpha|}}\left[\left(-2\mu+\frac{2\mu\phi_1-|\alpha|}{\phi_L-\phi_1}\right)\chi + \left(\frac{(2\mu\phi_1-|\alpha|)\phi_L}{\phi_1(\phi_L-\phi_1)}\right)\Pi\left(\arcsin\left(\mathrm{sn}(\chi,k)\right),\tilde{\alpha}_{10}^2,k\right)\right], \tag{4.4}$$

where $k^2=\frac{-\hat{\alpha}_{10}^2(2\mu\phi_L-|\alpha|)}{|\alpha|}$, $\hat{\alpha}_{10}^2=\frac{-\phi_M}{\phi_L}<0$, $\tilde{\alpha}_{10}^2=\frac{-\hat{\alpha}_{10}^2(\phi_L-\phi_1)}{\phi_1}$, and $\chi_{012}=\mathrm{sn}^{-1}\sqrt{\frac{\phi_L\phi_1}{(\phi_L-\phi_1)\phi_M}}$.

For the two homoclinic orbits defined by $H(\rho,y)=h_1$, enclosing the equilibria $E_2(\mp\rho_2,0)$ in Figure 9(b), we obtain:

$$\rho(\chi) = \mp\left(\phi_L-\frac{\phi_L-\frac{|\alpha|}{2\mu}}{1-\hat{\alpha}_{11}^2\mathrm{sn}^2(\chi,k)}\right)^{\frac{1}{2}}, \quad \chi\in(-\chi_{013},\chi_{013}),$$

$$\xi(\chi) = \frac{2}{\sqrt{(\phi_L-\phi_M)|\alpha|}}\left[\left(2\mu+\frac{2\mu\phi_1-|\alpha|}{\phi_L-\phi_1}\right)\chi + \left(\frac{(2\mu\phi_1-|\alpha|)(\phi_L-\frac{|\alpha|}{2\mu})}{(\frac{|\alpha|}{2\mu}-\phi_1)(\phi_L-\phi_1)}\right)\Pi\left(\arcsin\left(\mathrm{sn}(\chi,k)\right),\tilde{\alpha}_{11}^2,k\right)\right], \tag{4.5}$$

where $k^2=\frac{2\hat{\alpha}_{11}^2\mu\phi_L}{|\alpha|}$, $\hat{\alpha}_{11}^2=\frac{\frac{|\alpha|}{2\mu}-\phi_M}{\phi_L-\phi_M}$, $\tilde{\alpha}_{11}^2=\frac{\hat{\alpha}_{11}^2(\phi_L-\phi_1)}{\frac{|\alpha|}{2\mu}-\phi_1}$, and $\chi_{013}=\mathrm{sn}^{-1}\sqrt{\frac{\phi_L\phi_1}{(\phi_L-\phi_1)\phi_M}}$.

For the two open orbits in Figure 9(b) tending to the singular straight lines $\rho=\mp\rho_s$ as $|y|\to\infty$, we obtain two compacton solutions:

$$\rho(\chi) = \mp\left(\frac{\phi_L}{1-\hat{\alpha}_{12}^2\mathrm{sn}^2(\chi,k)}\right)^{\frac{1}{2}}, \quad \chi\in(-\chi_{014},\chi_{014}),$$

$$\xi(\chi) = \frac{2}{\sqrt{(\phi_L-\phi_M)|\alpha|}}\left[\left(4\mu-\frac{|\alpha|}{\phi_1}\right)\chi+\left(\frac{(2\mu\phi_1-|\alpha|)\phi_L}{\phi_1(\phi_L-\phi_1)}\right)\Pi\left(\arcsin\left(\mathrm{sn}(\chi,k)\right),\tilde{\alpha}_{12}^2,k\right)\right], \tag{4.6}$$

where $k^2=\frac{-\hat{\alpha}_{12}^2\phi_M}{\phi_L-\phi_M}$, $\hat{\alpha}_{12}^2=\frac{|\alpha|-2\mu\phi_L}{|\alpha|}<0$, $\tilde{\alpha}_{12}^2=\frac{-\hat{\alpha}_{12}^2\phi_1}{\phi_L-\phi_1}$, and $\chi_{014}=\mathrm{sn}^{-1}\sqrt{\frac{|\alpha|(\phi_L-\phi_3)}{(2\mu\phi_L-|\alpha|)\phi_3}}$.

4.2. The case $h_3<h_s=h_1<h_2<0$ in Figure 3(b).

(i) For the heteroclinic loop defined by $H(\rho,y)=h_1=h_s$ in Figure 9(c), enclosing the origin, we obtain the kink and anti-kink wave solutions:

$$\rho(\xi) = \mp\left(\frac{2\phi_1(\phi_M-\phi_1)}{\phi_M\cosh\left(\sqrt{\phi_1(\phi_M-\phi_1)}\xi\right)+(\phi_M-2\phi_1)}\right)^{\frac{1}{2}}. \tag{4.7}$$

(ii) For the two homoclinic orbits defined by $H(\rho,y)=h_1=h_s$ in Figure 9(c), passing through the singular straight lines $\rho = \mp\rho_s$, we have two solitary wave solutions:

$$\rho(\xi) = \mp\left(\phi_1 + \frac{2\phi_1(\phi_M - \phi_1)}{\phi_M \cosh\left(\sqrt{\phi_1(\phi_M - \phi_1)}\xi\right) - (\phi_M - 2\phi_1)}\right)^{\frac{1}{2}}. \tag{4.8}$$

When $\xi = \xi_{s1} = \frac{1}{\sqrt{\phi_1(\phi_M - \phi_1)}}\cosh^{-1}\left(\frac{|\alpha|(2\phi_1 - \phi_M) - 2\mu\phi_1(\phi_1 + \phi_M)}{(2\mu\phi_1 - |\alpha|)\phi_M}\right)$, we have $\rho(\xi_{s1}) = \mp\rho_s$.

(iii) For the two triangular orbits defined by $H(\rho, y) = h_1 = h_s$ in Figure 9(c), enclosing the equilibria $E_2(\mp\rho_2, 0)$, we obtain peakon and anti-peakon solutions (see Figure 10(c)):

$$\rho(\xi) = \mp\left(\phi_1 + \frac{2\phi_1(\phi_M - \phi_1)}{\phi_M \cosh\left(\sqrt{\phi_1(\phi_M - \phi_1)}|\xi|\right) - (\phi_M - 2\phi_1)}\right)^{\frac{1}{2}}, \quad \xi \in (-\infty, -\xi_{s1}) \cup (\xi_{s1}, \infty). \tag{4.9}$$

(iv) For the two arch orbits defined by $H(\rho, y) = h_1 = h_s$ in Figure 9(c), enclosing $E_3(\mp\rho_3, 0)$, we have two periodic peakon solutions:

$$\rho(\xi) = \mp\left(\phi_1 + \frac{2\phi_1(\phi_M - \phi_1)}{\phi_M \cosh\left(\sqrt{\phi_1(\phi_M - \phi_1)}|\xi|\right) - (\phi_M - 2\phi_1)}\right)^{\frac{1}{2}}, \quad \xi \in (-\xi_{s1}, \xi_{s1}). \tag{4.10}$$

4.3. The case $h_3 < h_1 < h_s < h_2 < 0$ in Figure 3(c).

The level curves defined by $H(\rho, y) = h_1$ and $H(\rho, y) = h_s$ are highlighted in Figures 11(a) and (b).

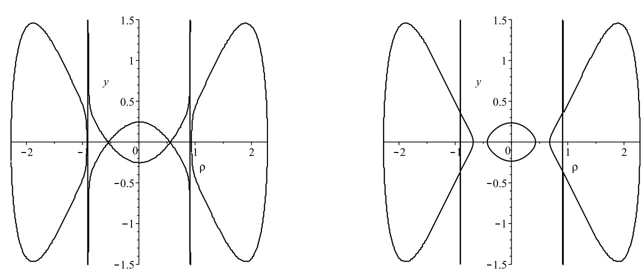

(a) $h = h_1$. (b) $h = h_s$.

Figure 11. Level curves of system (1.9) defined by $H(\rho, y) = h$ when $\alpha < 0, \mu > 0$.

(i) For the heteroclinic loop defined by $H(\rho, y) = h_1$ in Figure 11(a), enclosing the origin, we obtain the kink and anti-kink solutions:

$$\begin{aligned} \rho(\chi) &= \mp\left(\frac{-\phi_a\hat{\alpha}_{13}^2\mathrm{sn}^2(\chi, k)}{1 - \hat{\alpha}_{13}^2\mathrm{sn}^2(\chi, k)}\right)^{\frac{1}{2}}, \quad \chi \in (-\chi_{015}, \chi_{015}), \\ \xi(\chi) &= \mp\frac{2}{\sqrt{(2\mu\phi_a - |\alpha|)\phi_b}}\left[\left(-2\mu + \frac{2\mu\phi_1 - |\alpha|}{\phi_a - \phi_1}\right)\chi\right. \\ &\quad \left. + \left(\frac{(2\mu\phi_1 - |\alpha|)\phi_a}{\phi_1(\phi_a - \phi_1)}\right)\Pi\left(\arcsin\left(\mathrm{sn}(\chi, k)\right), \tilde{\alpha}_{13}^2, k\right)\right], \end{aligned} \tag{4.11}$$

where $k^2 = \frac{-\hat{\alpha}_{13}^2(\phi_a-\phi_b)}{\phi_b}$, $\hat{\alpha}_{13}^2 = \frac{-|\alpha|}{2\mu\phi_a-|\alpha|} < 0$, $\tilde{\alpha}_{13}^2 = \frac{-\hat{\alpha}_{13}^2(\phi_a-\phi_1)}{\phi_1}$, and $\chi_{015} = \mathrm{sn}^{-1}\sqrt{\frac{(2\mu\phi_a-|\alpha|)\phi_1}{(\phi_a-\phi_1)|\alpha|}}$.

(ii) For the two periodic orbits defined by $H(\rho, y) = h_1$ in Figure 11(a), enclosing $E_3(\mp\rho_3, 0)$, we obtain:

$$\rho(\chi) = \mp\left(\frac{|\alpha|}{2\mu} + \frac{\phi_b - \frac{|\alpha|}{2\mu}}{1-\hat{\alpha}_{14}^2\mathrm{sn}^2(\chi,k)}\right)^{\frac{1}{2}},$$

$$\xi(\chi) = \frac{2}{\sqrt{(2\mu\phi_a-|\alpha|)\phi_b}}\left[\left(2\mu + \frac{2\mu\phi_1-|\alpha|}{\frac{|\alpha|}{2\mu}-\phi_1}\right)\chi + \left(\frac{(2\mu\phi_1-|\alpha|)(\frac{|\alpha|}{2\mu}-\phi_b)}{(\frac{|\alpha|}{2\mu}-\phi_1)(\phi_b-\phi_1)}\right)\Pi\left(\arcsin\left(\mathrm{sn}(\chi,k)\right), \tilde{\alpha}_{14}^2, k\right)\right], \tag{4.12}$$

where $k^2 = \frac{\hat{\alpha}_{14}^2|\alpha|}{2\mu\phi_b}$, $\hat{\alpha}_{14}^2 = \frac{\phi_a-\phi_b}{\phi_a-\frac{|\alpha|}{2\mu}}$, and $\tilde{\alpha}_{14}^2 = \frac{\hat{\alpha}_{14}^2(\frac{|\alpha|}{2\mu}-\phi_1)}{\phi_b-\phi_1}$.

(iii) For the unique periodic orbit defined by $H(\rho, y) = h_s$ in Figure 11(b), enclosing the origin, we have:

$$\rho(\xi) = \mp\left|\frac{-\phi_M\hat{\alpha}_{15}^2\mathrm{sn}^2(\Omega_1\xi,k)}{1-\hat{\alpha}_{15}^2\mathrm{sn}^2(\Omega_1\xi,k)}\right|^{\frac{1}{2}}, \tag{4.13}$$

where $\hat{\alpha}_{15}^2 = \frac{-\phi_c}{\phi_M-\phi_c} < 0$, $k^2 = \frac{-\hat{\alpha}_{15}^2(\phi_M-\phi_m)}{\phi_m}$, and $\Omega_1 = \frac{1}{2}\sqrt{(\phi_M-\phi_c)\phi_m}$.

(iv) For the two closed orbits defined by $H(\rho, y) = h_s$ in Figure 11(b), passing through $\rho = \mp\rho_s$, we have:

$$\rho(\xi) = \mp\left(\frac{\phi_M}{1-\hat{\alpha}_{16}^2\mathrm{sn}^2(\Omega_1\xi,k)}\right)^{\frac{1}{2}}, \tag{4.14}$$

where $\hat{\alpha}_{16}^2 = 1 - \frac{\phi_M}{\phi_m} < 0$ and $k^2 = \frac{-\hat{\alpha}_{16}^2\phi_c}{\phi_M-\phi_c}$. When $\xi = \xi_{s2} = \mathrm{sn}^{-1}\sqrt{\frac{\phi_M(\phi_M-\phi_s)}{\phi_s(\phi_M-\phi_m)}}$, we have $\rho(\xi_{s2}) = \rho_s$.

(v) For the four arch orbits defined by $H(\rho, y) = h_s$ in Figure 11(b), which intersect the two singular lines $\rho = \mp\rho_s$, we have four periodic peakon solutions:

$$\rho(\xi) = \mp\left(\frac{\phi_M}{1-\hat{\alpha}_{16}^2\mathrm{sn}^2(\Omega_1\xi,k)}\right)^{\frac{1}{2}}, \quad \xi \in (-\xi_{s2}, \xi_{s2}) \tag{4.15}$$

and

$$\rho(\xi) = \mp\left(\frac{\phi_M}{1-\hat{\alpha}_{16}^2\mathrm{sn}^2(\Omega_1\xi,k)}\right)^{\frac{1}{2}}, \quad \xi \in (K(k)-\xi_{s2}, K(k)+\xi_{s2}), \tag{4.16}$$

where $K(k)$ is the complete elliptic integral of the first kind.

In summary, the following theorem is established.

Theorem 4.1. *Assume that $\alpha < 0, \mu > 0$ and the conditions of Theorem 2.1 hold. Then, system (1.9) admits the exact explicit parametric representations:*

(i) *Periodic wave solutions of the form $\rho(\xi)$ given by (4.1), (4.12), (4.13), and (4.14).*

(ii) *Sawtooth wave solutions of the form $\rho(\xi)$ given by (4.2).*

(iii) *Periodic peakon solutions of the form* $\rho(\xi)$ *given by* (4.3), (4.10), (4.15), *and* (4.16).

(iv) *Peakon solutions of the form* $\rho(\xi)$ *given by* (4.9).

(v) *Kink and anti-kink wave solutions of the form* $\rho(\xi)$ *given by* (4.7).

(vi) *Solitary wave solutions of the form* $\rho(\xi)$ *given by* (4.8).

(vii) *Solitary wave solutions of the form* $(\rho(\chi), \xi(\chi))$ *given by* (4.5).

(viii) *Kink and anti-kink wave solutions of the form* $(\rho(\chi), \xi(\chi))$ *given by* (4.4) *and* (4.11).

(ix) *Compacton solutions of the form* $(\rho(\chi), \xi(\chi))$ *given by* (4.6).

5. Exact parametric representations of bounded solutions for $\alpha > 0, \mu < 0$

In this section, we derive the exact parametric representations for the bounded traveling waves depicted in Figure 4.

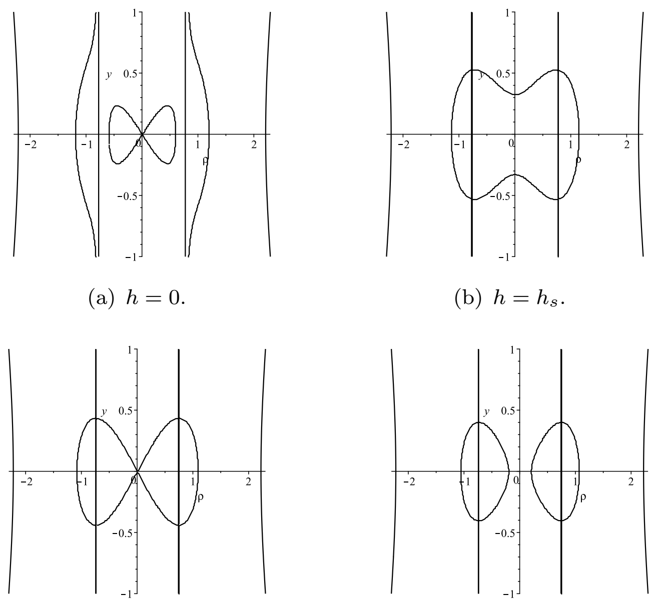

(a) $h = 0$. (b) $h = h_s$.

(c) $h = 0 = h_s$. (d) $h = h_s$.

Figure 12. Level curves of system (1.9) defined by $H(\rho, y) = h$ when $\alpha > 0, \mu < 0$.

5.1. The case $h_3 < h_1 < 0 < h_s < h_2$ in Figure 4(a).

The singular level curves defined by $H(\rho, y) = 0$ and $H(\rho, y) = h_s$ are shown in Figures 12(a) and (b).

(i) For the double homoclinic orbits defined by $H(\rho, y) = 0$ in Figure 12(a), each branch enclosing $E_1(\mp\rho_1, 0)$, we obtain:

$$\begin{aligned} \rho(\chi) &= \mp\left(\frac{\alpha}{2|\mu|} - \frac{\frac{\alpha}{2|\mu|} - \phi_M}{1 - \hat{\alpha}_{17}^2 \mathrm{sn}^2(\chi, k)}\right)^{\frac{1}{2}}, \quad \chi \in (-\chi_{017}, \chi_{017}), \\ \xi(\chi) &= \frac{2}{\sqrt{(2|\mu|\phi_a - \alpha)(\phi_b - \phi_M)}}\left(\frac{\alpha}{\phi_M} - 2|\mu|\right) \Pi\left(\arcsin\left(\mathrm{sn}(\chi, k)\right), \tilde{\alpha}_{17}^2, k\right), \end{aligned} \tag{5.1}$$

where $k^2=\frac{\hat{\alpha}_{17}^2(\phi_b-\frac{\alpha}{2|\mu|})}{\phi_b-\phi_M}$, $\hat{\alpha}_{17}^2=\frac{\phi_a-\phi_M}{\phi_a-\frac{\alpha}{2|\mu|}}$, $\tilde{\alpha}_{17}^2=\frac{\hat{\alpha}_{17}^2\alpha}{2|\mu|\phi_M}$, and $\chi_{017}=\mathrm{sn}^{-1}\sqrt{\frac{(2\mu\phi_a-|\alpha|)\phi_M}{(\phi_a-\phi_M)|\alpha|}}$.

(ii) For the two unbounded orbits defined by $H(\rho,y)=0$ that tend to $\rho=\mp\rho_s$ as $|y|\to\infty$ in Figure 12(a), we obtain two compacton solutions:

$$\rho(\chi)=\mp\left(\phi_a-\frac{\phi_a-\phi_b}{1-\hat{\alpha}_{18}^2\mathrm{sn}^2(\chi,k)}\right)^{\frac{1}{2}},\quad \chi\in(-\chi_{018},\chi_{018}),$$

$$\xi(\chi)=\frac{2}{\sqrt{(2|\mu|\phi_a-\alpha)(\phi_b-\phi_M)}}\left[\left(-\frac{\alpha}{\phi_a}+2|\mu|\right)\chi-\alpha\left(\frac{\phi_a-\phi_b}{\phi_a\phi_b}\right)\Pi\left(\arcsin\left(\mathrm{sn}(\chi,k)\right),\tilde{\alpha}_{18}^2,k\right)\right],\tag{5.2}$$

where $k^2=\frac{\hat{\alpha}_{18}^2(\phi_a-\phi_M)}{\phi_b-\phi_M}$, $\hat{\alpha}_{18}^2=\frac{\phi_b-\frac{\alpha}{2|\mu|}}{\phi_a-\frac{\alpha}{2|\mu|}}$, $\tilde{\alpha}_{18}^2=\frac{\hat{\alpha}_{18}^2\phi_a}{\phi_b}$, and $\chi_{018}=\mathrm{sn}^{-1}\sqrt{\frac{(2\mu\phi_a-|\alpha|)(\phi_b-\phi_s)}{(\phi_a-\phi_s)(2|\mu|\phi_b-\alpha)}}$.

(iii) For the closed orbits defined by $H(\rho,y)=h_s$ in Figure 12(b), passing through the singular lines $\rho=\mp\rho_s$, we have:

$$\rho(\xi)=\mp\left|-\phi_d+\frac{\phi_d}{1-\hat{\alpha}_{18}^2\mathrm{sn}^2(\Omega_2\xi,k)}\right|^{\frac{1}{2}},\tag{5.3}$$

where $\hat{\alpha}_{18}^2=\frac{\phi_M}{\phi_M+\phi_d}$, $k^2=\frac{\hat{\alpha}_{18}^2(\phi_a+\phi_d)}{\phi_a}$, and $\Omega_2=\frac{1}{2}\sqrt{\phi_a(\phi_M+\phi_d)}$. When $\xi=\xi_{s3}=\mathrm{sn}^{-1}\sqrt{\frac{\phi_s(\phi_M+\phi_d)}{\phi_M(\phi_s+\phi_d)}}$, we have $\rho(\xi_{s3})=\phi_s$.

(iv) For the two arch orbits defined by $H(\rho,y)=h_s$ in Figure 12(b), enclosing $E_2(\mp\rho_2,0)$, we obtain two periodic peakon solutions:

$$\rho(\xi)=\mp\left|-\phi_d+\frac{\phi_d}{1-\hat{\alpha}_{18}^2\mathrm{sn}^2(\Omega_2\xi,k)}\right|^{\frac{1}{2}},\quad \xi\in(K(k)-\xi_{s3},K(k)+\xi_{s3}).\tag{5.4}$$

(v) For the curve quadrilateral orbit defined by $H(\rho,y)=h_s$ in Figure 12(b), enclosing the origin, we have a sawtooth wave solution:

$$\rho(\xi)=\mp\left|-\phi_d+\frac{\phi_d}{1-\hat{\alpha}_{18}^2\mathrm{sn}^2(\Omega_2\xi,k)}\right|^{\frac{1}{2}},\quad \xi\in(-\xi_{s3},\xi_{s3}).\tag{5.5}$$

5.2. The case $h_3<h_1<0=h_s<h_2$ in Figure 4(b).

(i) For the two homoclinic orbits defined by $H(\rho,y)=0=h_s$ in Figure 12(c), enclosing $E_1(\mp\rho_1,0)$ and $E_3(\mp\rho_3,0)$, we have two solitary wave solutions:

$$\rho(\xi)=\mp\left(\frac{2\phi_L\phi_M}{(\phi_L-\phi_M)\cosh\left(\sqrt{\phi_L\phi_M}\xi\right)+(\phi_L+\phi_M)}\right)^{\frac{1}{2}}.\tag{5.6}$$

When $\xi=\xi_{s4}=\frac{1}{\sqrt{\phi_L\phi_M}}\cosh^{-1}\left(\frac{2\phi_M\phi_L-(\phi_L+\phi_M)\phi_s}{(\phi_L-\phi_M)\phi_s}\right)$, we have $\rho(\xi_{s4})=\rho_s$.

(ii) For the triangular orbits defined by $H(\rho,y)=0=h_s$ in Figure 12(c), enclosing $E_1(\mp\rho_1,0)$, we obtain peakon and anti-peakon solutions:

$$\rho(\xi)=\mp\left(\frac{2\phi_L\phi_M}{P_2\cosh_{q_2}\left(\sqrt{\phi_L\phi_M}\xi\right)-(\phi_L+\phi_M)}\right)^{\frac{1}{2}},\tag{5.7}$$

where $P_2=\frac{1}{\phi_s}\left(2\sqrt{\phi_L\phi_M X(\phi_s)}-(\phi_L+\phi_M)\phi_s+2\phi_L\phi_M\right)$ and $q_2=\frac{(\phi_L-\phi_M)^2}{P_2^2}$.

(iii) For the two arch orbits defined by $H(\rho, y) = 0 = h_s$ in Figure 12(c), enclosing $E_3(\mp\rho_3, 0)$, we obtain two periodic peakons:

$$\rho(\xi) = \mp\left(\frac{2\phi_L\phi_M}{(\phi_L - \phi_M)\cosh\left(\sqrt{\phi_L\phi_M}\xi\right) + (\phi_L + \phi_M)}\right)^{\frac{1}{2}}, \quad \xi \in (-\xi_{s4}, \xi_{s4}). \tag{5.8}$$

5.3. The case $h_3 < h_1 < h_s < 0 < h_2$ in Figure 4(c).

(i) For the two closed orbits defined by $H(\rho, y) = h_s$ in Figure 12(d), enclosing $E_1(\mp\rho_1, 0)$ and $E_3(\mp\rho_3, 0)$, we have two periodic wave solutions:

$$\rho(\xi) = \mp\left(\phi_L - \frac{\phi_L - \phi_M}{1 - \hat{\alpha}_{18}^2\mathrm{sn}^2(\Omega_3\xi, k)}\right)^{\frac{1}{2}}, \tag{5.9}$$

where $\hat{\alpha}_{18}^2 = \frac{\phi_M - \phi_m}{\phi_L - \phi_m}$, $k^2 = \frac{\hat{\alpha}_{18}^2\phi_L}{\phi_M}$, and $\Omega_3 = \frac{1}{2}\sqrt{(\phi_L - \phi_m)phi_M}$. Notably, when $\xi = \xi_{s5} = \frac{1}{\Omega_3}\mathrm{sn}^{-1}\sqrt{\frac{(\phi_M - \phi_s)(\phi_L - \phi_m)}{(\phi_L - \phi_s)(\phi_M - \phi_m)}}$, we have $\rho(\xi_{s5}) = \rho_s$.

(ii) For the two arch orbits defined by $H(\rho, y) = h_s$ in Figure 12(d), enclosing two singular points $E_3(\mp\rho_3, 0)$, respectively, we obtain four periodic peakon solutions:

$$\rho(\xi) = \mp\left(\phi_L - \frac{\phi_L - \phi_M}{1 - \hat{\alpha}_{18}^2\mathrm{sn}^2(\Omega_3\xi, k)}\right)^{\frac{1}{2}}, \quad \xi \in (-\xi_{s5}, \xi_{s5}), \tag{5.10}$$

and

$$\rho(\xi) = \mp\left(\phi_L - \frac{\phi_L - \phi_M}{1 - \hat{\alpha}_{18}^2\mathrm{sn}^2(\Omega_3\xi, k)}\right)^{\frac{1}{2}}, \quad \xi \in (K(k) - \xi_{s5}, K(k) + \xi_{s5}). \tag{5.11}$$

In summary, the following theorem is established.

Theorem 5.1. *Assume that $\alpha > 0, \mu < 0$ and the conditions of Theorem 2.1 hold. Then, system* (1.9) *admits the exact explicit parametric representations:*

(i) *Periodic wave solutions of the form $\rho(\xi)$ given by* (5.3) *and* (5.9).

(ii) *Sawtooth wave solutions of the form $\rho(\xi)$ given by* (5.5).

(iii) *Periodic peakon solutions of the form $\rho(\xi)$ given by* (5.4), (5.10), *and* (5.11).

(iv) *Peakon solutions of the form $\rho(\xi)$ given by* (5.7).

(v) *Solitary wave solutions of the form $\rho(\xi)$ given by* (5.6).

(vi) *Solitary wave solutions of the form $(\rho(\chi), \xi(\chi))$ given by* (5.1).

(vii) *Compacton solutions of the form $(\rho(\chi), \xi(\chi))$ given by* (5.2).

6. Conclusion and discussion

In this paper, we have systematically investigated the bifurcations and exact bounded traveling wave solutions of a higher-order nonlinear Schrödinger equation with seventh-order polynomial nonlinearity and weak nonlocality. By reducing the governing PDE to a planar Hamiltonian dynamical system, we established a systematic topological classification of its phase portraits under different parameter regimes and derived more than 42 distinct families of exact bounded traveling wave solutions, including smooth periodic and solitary waves, kink and anti-kink waves, peakons, periodic peakons, sawtooth waves, and compactons. From the optical perspective, these solutions represent different propagation regimes in weakly nonlocal nonlinear media: Solitary waves correspond to localized pulses sustained by the balance between diffraction and high-order nonlinear effects, kink and anti-kink waves describe transitions between distinct continuous-wave backgrounds, while smooth periodic waves represent spatially modulated wave trains. The non-smooth solutions arise naturally in the singular regimes $\mu\alpha < 0$, where the traveling-wave system possesses singular straight lines. In particular, peakons and periodic peakons exhibit finite jumps in their first derivatives at the peaks, whereas compactons possess strictly compact support. Thus, the phase-portrait analysis not only provides a unified dynamical-systems framework for the construction of these solutions, but also reveals the connection between the parameter-dependent geometry of the reduced Hamiltonian system and the diversity of optical wave structures supported by the original equation.

The non-smooth traveling wave profiles obtained in Sections 4 and 5 should be understood as piecewise classical solutions, with their behavior across the singular lines interpreted in the appropriate weak or distributional sense. At a peak, the amplitude remains continuous while its first derivative undergoes a finite jump, with the one-sided derivatives satisfying the corresponding symmetry condition; for compactons, the profile and its first derivative vanish at the boundaries of the compact support, allowing the wave to be matched continuously with the zero background. The consistency of the analytical representations was further checked through direct substitution into the first integral $H(\rho, y) = h$ and numerical residual tests for representative parameter sets, providing an independent verification of the derived formulas. These results demonstrate that the singular traveling-wave framework is capable of describing a substantially richer class of exact structures than conventional smooth traveling-wave analysis. Several questions remain open. In particular, the case $C \neq 0$, corresponding to nontrivial phase chirp and a singular term at $\rho = 0$, requires a separate analysis because the corresponding traveling-wave system has a fundamentally different singular structure. Moreover, the orbital stability and spectral stability of the obtained solitary waves and multi-peakon configurations, as well as the persistence and interactions of these structures under perturbations, constitute important directions for future investigation.

References

[1] A. Arai, *Exactly solvable supersymmetric quantum mechanics*, J. Math. Anal. Appl., 1991, 158(1), 63–79.

[2] A. Arai, *Exact solutions of multi-component nonlinear Schrödinger and Klein–Gordon equations in two-dimensional space–time*, J. Phys. A: Math. Gen., 2001, 34(21), 4281–4288.

[3] P. F. Byrd and M. D. Friedman, *Handbook of Elliptic Integrals for Engineers and Scientists*, Springer, Berlin, 1971.

[4] R. Camassa and D. D. Holm, *An integrable shallow water equation with peaked solitons*, Phys. Rev. Lett., 1993, 71(8), 1661–1664.

[5] R. Camassa, J. M. Hyman and B. P. Luce, *Nonlinear waves and solitons in physical systems*, Physica D, 1998, 123(1), 1–20.

[6] P. W. M. Chin, *The existence of the global solution of the semi-linear Schrödinger equation with numerical computation on the Dirichlet boundary*, J. Appl. Anal. Comput., 2025, 15(2), 786–809.

[7] A. Degasperis, D. D. Holm and A. N. W. Hone, *A new integrable equation with peakon solutions*, Theoret. Math. Phys., 2002, 133(3), 1463–1474.

[8] A. Degasperis and M. Procesi, *Asymptotic integrability*, in: A. Degasperis, G. Gaeta (Eds.), Symmetry and Perturbation Theory, World Scientific, Singapore, 1999, 23–37.

[9] A. S. Fokas, *On a class of physically important integrable equations*, Physica D, 1995, 87(2–4), 145–150.

[10] W. Geng, M. Han, Y. Tian and A. Ke, *Heteroclinic bifurcation of limit cycles in perturbed cubic Hamiltonian systems by higher-order analysis*, J. Differential Equations, 2023, 357, 412–435.

[11] M. Han, *On the uniqueness of limit cycles in codimension two bifurcations*, J. Nonlinear Model. Anal., 2024, 6(3), 509–530.

[12] M. Han, A. Ke, *On symmetry property of center manifolds of differential systems*, J. Appl. Anal. Comput., 2025, 15(1), 1–8.

[13] M. Han, J. Yang and J. Li, *General study on limit cycle bifurcation near a double homoclinic loop*, J. Differential Equations, 2023, 347, 1–23.

[14] D. He, K. Zhang and S. Tang, *Orbital stability of the sum of N peakons for the CH-mCH equation*, J. Nonlinear Model. Anal., 2025, 7(3), 794–822.

[15] R. O. de Jesus, C. A. Raposo, J. O. Ribeiro and O. V. Villagran, *Timoshenko system with internal dissipation of fractional derivative type*, J. Appl. Anal. Comput., 2025, 15(2), 1146–1169.

[16] J. Li, *Singular Nonlinear Traveling Wave Equations: Bifurcations and Exact Solutions*, Science Press, Beijing, 2013.

[17] J. Li and G. Chen, *On a class of singular nonlinear traveling wave equations*, Int. J. Bifurcation Chaos, 2007, 17(11), 4049–4065.

[18] J. Li and Z. Qiao, *Peakon, pseudo-peakon, and cuspon solutions for two generalized Camassa-Holm equations*, J. Math. Phys., 2013, 54(12), 123501.

[19] J. Li and Z. Shi, *Traveling wave solutions of some abcd-water wave models describing small amplitude, long wavelength gravity waves on the surface of water*, J. Nonlinear Model. Anal., 2025, 7(3), 1125–1141.

[20] J. Li, Q. Yu and Q. Zhang, *Unfolding a Hopf bifurcation in a linear reaction-diffusion equation with strongly localized impurity*, J. Appl. Anal. Comput., 2025, 15(3), 1742–1769.

[21] J. Li, W. Zhou and G. Chen, *Understanding peakons, periodic peakons and compactons via a shallow water wave equation*, Int. J. Bifurcation Chaos, 2016, 26(4), 1650207.

[22] F. Liang and M. Han, *Expansion coefficients and their relation for Melnikov functions near polycycles*, J. Differential Equations, 2025, 435, 113312.

[23] S. Liu and M. Han, *Bifurcation theory of limit cycles by higher order Melnikov functions and applications*, J. Differential Equations, 2024, 403, 29–66.

[24] W. Liu and M. Han, *Bifurcations of traveling wave solutions of a generalized Burgers–Fisher equation*, J. Math. Anal. Appl., 2024, 533(2), 128012.

[25] J. Llibre and X. Sun, *Small-amplitude periodic solutions in the polynomial jerk equation of arbitrary degree*, Physica D, 2025, 476, 134628.

[26] A. Messouber, H. Triki, X. Liu, A. Biswas, Y. Yildirim, A. Alghamdi and Q. Zhou, *Chirped spatial solitons on a continuous-wave background in weak nonlocal media with polynomial law of nonlinearity*, Phys. Lett. A, 2023, 467, 128731.

[27] V. Novikov, *Generalizations of the Camassa-Holm equation*, J. Phys. A: Math. Theor., 2009, 42(34), 342002.

[28] Z. Qiao, *A new integrable equation with cuspons and W/M-shape-peaks solitons*, J. Math. Phys., 2006, 47(11), 112701.

[29] Z. Qiao, *New integrable hierarchy, parametric solutions, cuspons, one-peak solitons, and M/W-shape peak solutions*, J. Math. Phys., 2007, 48(8), 082701.

[30] M. Singh, S. Das, Rajeev and E. M. Craciun, *Numerical simulation of variable order fractional coupled FitzHugh-Nagumo reaction-diffusion problem and its analysis*, J. Appl. Anal. Comput., 2025, 15(2), 810–838.

[31] X. Sun, G. Ji and Q. Bin, *Heteroclinic bifurcation near a loop tangent to an invariant line*, J. Differential Equations, 2025, 449, 113713.

[32] X. Sun, Y. Tian and M. Han, *Homoclinic bifurcation near a loop tangent to an invariant line*, J. Differential Equations, 2025, 425, 157–189.

[33] X. Sun, P. Yu and M. Zhang, *Melnikov analysis in the complex cubic-quintic Ginzburg-Landau equation with higher-order dispersion*, Physica D, 2026, 494, 135260.

[34] X. Sun and M. Zhang, *Dynamics of a quartic Korteweg–de Vries equation with multiple dissipations via an Abelian integral approach*, Chaos, 2025, 35(8), 083118.

[35] Q. Wang, N. Wang and X. Sun, *Monotonicity of the ratios of two Abelian integrals for Hamiltonian systems with parameters*, J. Appl. Anal. Comput., 2024, 14(5), 2466–2487.

[36] J. Yang and M. Han, *Limit cycles near a compound cycle in a near-Hamiltonian system with smooth perturbations*, Chaos Solitons Fractals, 2024, 184, 114963.

[37] Q. Zhou, D. Yao, S. Ding and Y. Zhang, *Spatial optical solitons in fifth order and seventh order weakly nonlocal nonlinear media*, Optik, 2013, 124(23), 5683–5686.

Received February 2025; Accepted August 2026; Available online September 2026.